Chapter 6

Adaptive Step-Size Orthogonal Gradient-Based Per-Tone Equalisation in Discrete Multitone Systems

Suchada Sitjongsataporn

Additional information is available at the end of the chapter

http://dx.doi.org/10.5772/52158

1. Introduction

An all-digital implementation of multicarrier modulation called *discrete multitone (DMT) modulation* has been standardised for asymmetric digital subscriber line (ADSL), ADSL2, ADSL2+ and VDSL [1]- [3]. ADSL modems rely on DMT modulation, which divides a broadband channel into many narrowband subchannels and modulated encoded signals onto the narrowband subchannels [4], [5]. With advanced digital signal processing algorithms, DMT system is to fight the impairments for wired communications such DSL-based technology. The major impairments such as the intersymbol interference (ISI), the intercarrier interference (ICI), the channel distortion, echo, radio-frequency interference (RFI) and crosstalk from DSL systems are induced as a result of large bandwidth utilisation over the telephone line. However, the improvement can be achieved by the equalisation concepts.

ISI and ICI caused by the length of channel impulse response can be eliminated by the use of cyclic prefix (CP) adding a copy of the last ν time-domain samples between DMT-symbols at the part of transmitter. The conventional equalisation in DMT-based systems consists of a (real) time-domain equaliser (TEQ) and the (complex) one-tap frequency-domain equalisers [6]. For a more sophisticated equalisation technique, a frequency-domain equaliser (FEQ) for each tone, called *per-tone equaliser (PTEQ)* has been introduced in order to give the bit rate maximising compared with existing equalisation schemes [7], [8].

The basic structure of the DMT transceiver is shown in Fig.1. The incoming bit stream is likewise reshaped to a complex-valued transmitted symbol for mapping in quadrature amplitude modulation (QAM). Then, the output of QAM bit stream is split into N parallel bit streams that are instantaneously fed to the modulating inverse fast Fourier transform (IFFT). After that, IFFT outputs are transformed into the serial symbols including the cyclic prefix between symbols and then fed to the channel. The transmitted signal sent over

the channel with impulse response is generally corrupted by the additive white Gaussian noise and near-end crosstalk. The received signal is also equalised by PTEQs without TEQ concerned. The per-tone equalisation structure is based on transferring the TEQ-operations into the frequency-domain after FFT demodulation, which results in a multitap PTEQ for each tone separately. Then, the parallel of received symbols are eventually converted into serial bits in the frequency-domain.

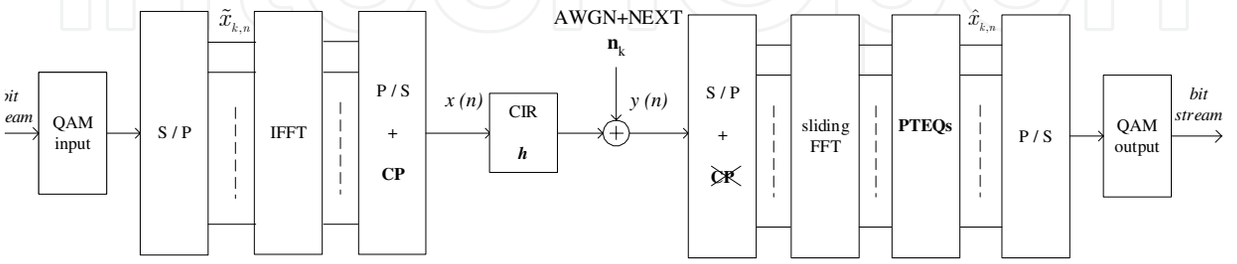

Figure 1. Block Diagram of a Discrete Multitone System.

It is a well known issue that in DMT theory, there is no overlapping between tones due to orthogonality derived from the discrete Fourier transformation among them. In practice, frequency-selective fading channel generally destroys such orthogonal structure leading to information interfering from adjacent tones as commonly known as ICI. In such case, information supposedly belonging to a particular tone generally smear into adjacent tones and leave some residual energy in them. The idea of a mixed-tone PTEQ for DMT-based system has been proposed in [9]. By recovering adaptively the knowledge of residual interfering signal energy from adjacent tones, the mixed-tone exponentially weighted least squares criterion can be shown to offer an improved signal to noise ratio (SNR) of the tone of interest.

In order to improve the convergence properties, the orthogonal gradient adaptive (OGA) has been presented by introducing orthogonal projection to the filtered gradient adaptive (FGA) algorithm. When the forgetting-factor is optimised sample by sample whereas a fixed forgetting-factor is used for FGA algorithm [10]. A normalised version of the OGA (NOGA) algorithm that has been introduced with the mixed-tone cost function and fixed step-size presented in [11]. With the purpose of the good tracking behaviour and recovering to a steady-state, it is necessary to let the step-size automatically track the change of system. Consequently, the concept of low complexity adaptive step-size approach based on the FGA algorithm is introduced for the per-tone equalisation in DMT-based systems in [12].

In this chapter, the focus is therefore to present low complexity orthogonal gradient-based algorithms for PTEQ based on the adaptive step-size approaches related to the mixed-tone criterion. The convergence behaviour and stability analysis of proposed algorithms will be investigated based on the mixed-tone weight-estimated errors. The convergence analysis of mechanisms will be carried out the steady-state and mean-square expressions of adaptive step-size parameter relating to the mean convergence factor.

http://dx.doi.org/10.5772/52158

2. System model and notation

In this section, the basic structure of the DMT transceiver is illustrated in Fig. 1. We describe that the data model and notation based on an FIR model of the DMT transmission channel is presented as [7]

$$\mathbf{y} = \mathbf{H}\cdot\mathbf{X} + \mathbf{n}\ ,$$

$$\underbrace{\begin{bmatrix} y_{k,l+\Delta} \\ \vdots \\ y_{k,N-l+\Delta} \end{bmatrix}}_{\mathbf{y}_{k,l+\Delta:N-1+\Delta}} = \underbrace{\left[\begin{array}{c|c|c} & [\,\bar{\mathbf{h}}^T\,]\ 0\ \cdots & \\ \mathbf{0}_{(1)} & \ddots\ \ddots & \mathbf{0}_{(2)} \\ & \cdots\ 0\ [\,\bar{\mathbf{h}}^T\,] & \end{array}\right] \cdot \begin{bmatrix} \mathcal{P}_\nu & \mathbf{0} & \mathbf{0} \\ \mathbf{0} & \mathcal{P}_\nu & \mathbf{0} \\ \mathbf{0} & \mathbf{0} & \mathcal{P}_\nu \end{bmatrix} \cdot \begin{bmatrix} \mathcal{I}_N & \mathbf{0} & \mathbf{0} \\ \mathbf{0} & \mathcal{I}_N & \mathbf{0} \\ \mathbf{0} & \mathbf{0} & \mathcal{I}_N \end{bmatrix} \cdot}_{\mathbf{H}}$$

$$\underbrace{\begin{bmatrix} \mathbf{x}_{k-1,N} \\ \mathbf{x}_{k,N} \\ \mathbf{x}_{k+1,N} \end{bmatrix}}_{\mathbf{X}_{k-1:k+1,N}} + \underbrace{\begin{bmatrix} \eta_{k,l+\Delta} \\ \vdots \\ \eta_{k,N-l+\Delta} \end{bmatrix}}_{\boldsymbol{\eta}_{k,l+\Delta:N-1+\Delta}} . \tag{1}$$

where l denotes as the first considered sample of the k-th received DMT-symbol. This depends on the number of tap of equaliser ($\mathbb{T}$) and the synchronisation delay (Δ). The vector $\mathbf{y}_{k,i:j}$ of received samples i to j of k-th DMT-symbol is as $\mathbf{y}_{k,i:j} = [y_{k,i} \ \cdots \ y_{k,j}]^T$. A sequence of the $N \times 1$ $\mathbf{x}_{k,N}$ transmitted symbol vector is as $\mathbf{x}_{k,N} = [x_{k,0} \ \cdots \ x_{k,N-1}]^T$. The size N is of inverse discrete Fourier transform (IDFT) and DFT. The parameter ν denotes as the length of cyclic prefix. The matrices $\mathbf{0}_{(1)}$ and $\mathbf{0}_{(2)}$ are also the zero matrices of size $(N-l)\times(N-L+2\nu+\Delta+l)$ and $(N-l)\times(N+\nu-\Delta)$. The vector $\bar{\mathbf{h}}$ is the $\mathbf{h}$ channel impulse responce (CIR) vector in reverse order. The $(N+\nu)\times N$ matrix $\mathcal{P}_\nu$ is denoted by

$$\mathcal{P}_\nu = \left[\begin{array}{c|c} \mathbf{0}_{\nu\times(N-\nu)} & \mathbf{I}_\nu \\ \hline & \mathbf{I}_N \end{array}\right] ,$$

which adds the cyclic prefix. The $\mathcal{I}_N$ is $N \times N$ IDFT matrix and modulates the input symbols. The $\boldsymbol{\eta}_{k,l+\Delta:N-1+\Delta}$ is a vector with additive white Gaussian noise (AWGN) and near-end cross-talk (NEXT).

Some notation will be used throughout this chapter as follows: $E\{\cdot\}$ is the expectation operator and diag$(\cdot)$ is a diagonal matrix operator. The operators $(\cdot)^T$, $(\cdot)^H$, $(\cdot)^*$ denote as the transpose, Hermitian and complex conjugate operators, respectively. The parameter k is the DMT symbol index and $\mathbf{I}_a$ is an $a \times a$ identity matrix. A tilde over the variable indicates the frequency-domain. The vectors are in bold lowercase and matrices are in bold uppercase.

3. Per-tone equalisation

In this section, we show the concept of per-tone equaliser (PTEQ). We refer the readers to [7] for more details. The per-tone equalisation structure is based on transferring the

TEQ-operations into the frequency-domain after DFT demodulation, which results in a $\mathbb{T}$-tap PTEQ for each tone separately. For each tone i ($i = 1 \ldots n$), the TEQ-operations are shown as follows [7]

$$\tilde{d}_n = \overbrace{\tilde{z}_n}^{\text{1-tap PTEQ}} \cdot \text{row}_n \overbrace{(\mathcal{F}_N) \cdot (\mathbf{Y} \cdot \mathbf{w})}^{\text{1 DFT}}, \tag{2}$$

$$= \text{row}_n \underbrace{(\mathcal{F}_N \cdot \mathbf{Y})}_{\mathbb{T}\text{ DFTs}} \cdot \underbrace{\mathbf{w} \cdot \tilde{z}_n}_{\mathbb{T}-\text{tap PTEQ } \mathbf{v}_n}, \tag{3}$$

where $\tilde{d}_n$ is the output after frequency-domain equalisation for tone n. The $\tilde{z}_n$ is the (complex) one-tap PTEQ for tone n. The parameter $\mathbf{w}$ is of (real) $\mathbb{T}$-tap TEQ and $\mathcal{F}_N$ is an $N \times N$ DFT matrix [7]. Note that $\mathbf{Y}$ is an $N \times \mathbb{T}$ Toeplitz matrix of received signal samples as vector $\mathbf{y}$ in (1). From (3), the $\mathbb{T}$ DFT-operations are cheaply calculated by means of a sliding DFT. It is demonstrated in [7] that every $\mathbb{T}$-tap PTEQ $\mathbf{v}_n$ exists a $\mathbb{T}$-tap PTEQ $\tilde{\mathbf{p}}_n$ which consists of only one DFT and $\mathbb{T} - 1$ real difference terms as its input.

The PTEQ output $\hat{x}_{k,n}$ can be specified as follows

$$\hat{x}_{k,n} = \tilde{\mathbf{p}}_n^H \cdot \underbrace{\left[\begin{array}{c|c|c} \mathbf{I}_{\mathbb{T}-1} & \mathbf{0} & \text{-}\mathbf{I}_{\mathbb{T}-1} \\ \hline \mathbf{0} & \multicolumn{2}{c}{\mathcal{F}_N(n,:)} \end{array}\right]}_{\mathbf{F}_n} \cdot \mathbf{y}, \tag{4}$$

$$= \tilde{\mathbf{p}}_n^H \cdot \tilde{\mathbf{y}}_{k,n}, \tag{5}$$

where $\tilde{\mathbf{p}}_n$ is the $\mathbb{T}$-tap complex-valued PTEQ vector for tone n. The $\mathbf{F}_n$ is a $(\mathbb{T}-1) \times (N + \mathbb{T} - 1)$ matrix [7]. The $\mathcal{F}_N(n,:)$ is the n^{th} row of $\mathcal{F}_N$. By using the sliding DFT, the first block row of matrix $\mathbf{F}_n$ in (4) extracts the difference terms, while the last row corresponds to the usual DFT operation as detailed in [7] and [13]. The vector $\mathbf{y}$ is of channel output samples as described in (1). The $\tilde{\mathbf{y}}_{k,n}$ is the sliding DFT output for tone n at each symbol k.

4. A mixed-tone cost function

In this section, we describe a mixed-tone cost function by means of the orthogonal projection matrix. The idea of using orthogonal projection of adjacent equalisers to include the information of interfering tones has been presented firstly in [9]. The illustration of the vector $\hat{\mathbf{p}}_m$ and its orthogonal projection as well as $\tilde{\mathbf{x}}_m$ for 2-dimensional subspace S^2 is shown in Fig. 2. The error vector $\mathbf{e}_m^{\perp}$ associated with the orthogonal projection of vectors $\hat{\mathbf{p}}_m$ and $\Pi_m^{\perp}\hat{\mathbf{p}}_m$, where $\Pi_m^{\perp}$ denotes as the orthogonal projection matrix of $\hat{\mathbf{p}}_m(k)$, will be presented in the update of the vector $\hat{\mathbf{p}}_m(k)$ where $k \neq m$. Therefore, the mixed-tone cost function derived as the sum of weight-estimated errors is optimised in order to achieve the solutions for frequency-domain equalisation. It is designed to work in conjunction with the complex-valued frequency-domain equalisation structure.

http://dx.doi.org/10.5772/52158

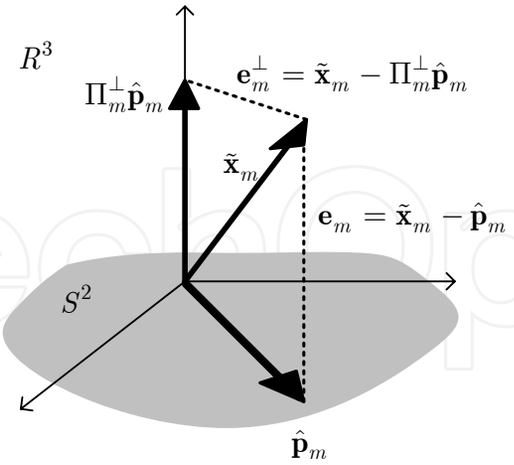

Figure 2. The tap-weight estimated PTEQ vector $\hat{\mathbf{p}}_m$ and its orthogonal projection $\Pi_m^{\perp}\hat{\mathbf{p}}_m$ are illustrated in two dimentional subspace S^2 [9].

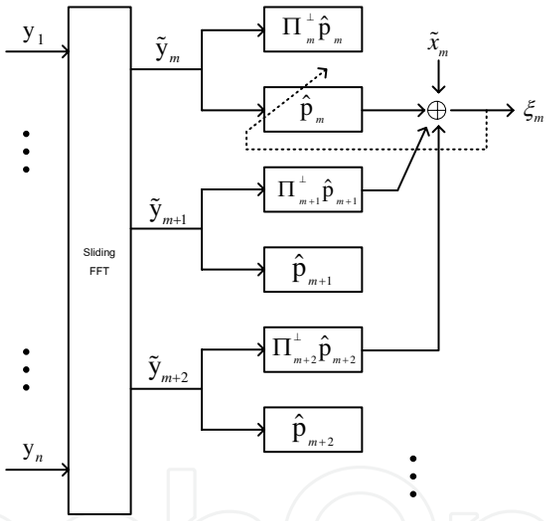

Figure 3. Block structure of the proposed mixed-tone PTEQ $\hat{\mathbf{p}}_m$ for $m \in M$ with the use of combining estimates of M-adjacent tones, where $M = 3$. [11]

A mixed-tone exponentially weighted least squares cost function to be minimised is defined as

$$J(k) = \frac{1}{2}\sum_{m=1}^{M}\sum_{i=1}^{k}\lambda_m^{k-i}\{\xi_m(i)\}^2, \tag{6}$$

where λ_m is the forgetting-factor and $\xi_m(k)$ is the mixed-tone weight-estimated error at tone m for $m \in M$. The number of the adjacent tones M is of tone of interest.

$$\begin{aligned}\xi_m(i) = \tilde{x}_m(i) - \hat{\mathbf{p}}_m^H(k)\tilde{\mathbf{y}}_m(i) - \left(\Pi_l^{\perp}(k)\hat{\mathbf{p}}_l(k)\right)^H\tilde{\mathbf{y}}_l(i) \\ - \left(\Pi_{l+1}^{\perp}(k)\hat{\mathbf{p}}_{l+1}(k)\right)^H\tilde{\mathbf{y}}_{l+1}(i) \\ - \ldots - \left(\Pi_L^{\perp}(k)\hat{\mathbf{p}}_L(k)\right)^H\tilde{\mathbf{y}}_L(i)\ , \\ \text{for } m \neq l\ ,\ L \leq M-1. \end{aligned} \tag{7}$$

where the parameter $\tilde{x}_m(k)$ is the k^{th} transmitted DMT-symbol on tone m. The vector $\hat{\mathbf{p}}_m(k)$ is of complex-valued $\mathbb{T}$-tap PTEQ for tone m. The vector $\tilde{\mathbf{y}}_m(k)$ is the DFT output for tone m at symbol k.

The orthogonal projection matrix $\Pi_l^{\perp}(k)$ which is the matrix difference determined by the tap-weight estimated vector $\hat{\mathbf{p}}_l(k)$ as [14]

$$\begin{aligned}\Pi_l^{\perp}(k) &= \tilde{\mathbf{I}} - \hat{\Pi}_l(k) \\ &= \tilde{\mathbf{I}} - \hat{\mathbf{p}}_l(k)\left[\hat{\mathbf{p}}_l^H(k)\,\hat{\mathbf{p}}_l(k)\right]^{-1}\hat{\mathbf{p}}_l^H(k)\ ,\end{aligned} \tag{8}$$

where $\tilde{\mathbf{I}}$ denotes as an identity matrix and $\hat{\Pi}_l(k)$ is the projection matrix onto the space spanned by the tap-weight vector $\hat{\mathbf{p}}_l(k)$. We note that the orthogonal projection matrix $\Pi_l^{\perp}(k)$ is mentioned by the vector $\hat{\mathbf{p}}_l(k)$ for $l \neq m$.

With the definition for this cost function, the m^{th}-term on the right hand side of (9) represents as the estimated mixed-tone error of the symbol k due to the m^{th}-tone of equaliser $\hat{\mathbf{p}}_m(k)$ for $m \in M$ as depicted in Fig. 3.

$$\xi_m(i) = \tilde{x}_m(i) - \hat{\mathbf{p}}_m^H(k)\tilde{\mathbf{y}}_m(i) - \sum_{l=1}^{L}\left(\Pi_l^{\perp}(k)\hat{\mathbf{p}}_l(k)\right)^H\tilde{\mathbf{y}}_l(i)\ ,\ \text{for } m \neq l\ ,\ L \leq M-1. \tag{9}$$

5. Adaptive step-size normalised orthogonal gradient adaptive algorithms

Based on filtered gradient adaptive algorithm, adaptive algorithms employing orthogonal gradient filtering can provide with the development of simple and robust filter across a wide range of input environments. This section is therefore concerned with the development of simple and robust adaptive frequency-domain equalisation by defining normalised orthogonal gradient adaptive algorithm.

In this section, we describe the orthogonal gradient adaptive (OGA) algorithm that is a class of the filtered gradient adaptive (FGA) algorithm using an orthogonal constraint. This employs the mixed-tone criterion described above in Section 4 in order to improve the convergence speed presented in Section 5.1, respectively.

The idea for low complexity adaptive step-size algorithms with the mixed-tone cost function is described in Section 5.2. For a large prediction error, the algorithm will increase the step-size to track the change of system whereas a small error will result in the decreased step-size [15], [16].

http://dx.doi.org/10.5772/52158

5.1. A Mixed-Tone Normalised Orthogonal Gradient Adaptive (MT-NOGA) algorithm

The orthogonal gradient adaptive (OGA) algorithm is formulated from the FGA algorithm [10] by introducing an orthogonal constraint between the present and previous direction vectors [17]. This OGA algorithm employs the optimised forgetting-factor on a sample-by-sample basis, so that the direction vector is orthogonal to the previous direction vector.

We then demonstrate the derivation of the mixed-tone normalised orthogonal gradient adaptive (MT-NOGA) algorithm for PTEQ in DMT-based systems. With this mixed-tone criterion in Section 4, the tap-weight estimate vector $\hat{\mathbf{p}}_m(k)$ at symbol k for $m \in M$ is given adaptively as

$$\hat{\mathbf{p}}_m(k) = \hat{\mathbf{p}}_m(k-1) + \mu_m(k)\,\mathbf{d}_m(k)\ , \tag{10}$$

where $\mu_m(k)$ is the step-size parameter and $\mathbf{d}_m(k)$ is the $\mathbb{T} \times 1$ direction vector.

The direction vector $\mathbf{d}_m(k)$ can be obtained recursively as

$$\begin{aligned}\mathbf{d}_m(k) &= \lambda_m(k)\,\mathbf{d}_m(k-1) + \mathbf{g}_m(k)\\ &= \lambda_m(k)\,\mathbf{d}_m(k-1) - \nabla_{\hat{\mathbf{p}}_m(k)} J(k)\ ,\end{aligned} \tag{11}$$

where $\mathbf{g}_m(k)$ is the negative gradient of cost function $J(k)$ in (6) and $\lambda_m(k)$ is the forgetting-factor at symbol k.

By differentiating $J(k)$ in (6) with respect to $\hat{\mathbf{p}}_m(k)$, we then get the gradient vector $\mathbf{g}_m(k)$ as

$$\begin{aligned}\mathbf{g}_m(k) &= -\nabla_{\hat{\mathbf{p}}_m(k)} J(k)\\ &= -\xi_m(k)\,\frac{\partial \xi_m(k)}{\partial \hat{\mathbf{p}}_m(k)} = \tilde{\mathbf{y}}_m(k)\,\xi_m^*(k)\ .\end{aligned} \tag{12}$$

where $\xi_m(k)$ is the *a priori* mixed-tone weight-estimated error at symbol k for $m \in M$ as

$$\xi_m(k) = \tilde{x}_m(k) - \hat{\mathbf{p}}_m^H(k-1)\tilde{\mathbf{y}}_m(k) - \sum_{l=1}^{L} \left(\Pi_l^{\perp}(k)\hat{\mathbf{p}}_l(k)\right)^H \tilde{\mathbf{y}}_l(k)\ ,\ \text{for } m \neq l\ ,\ L \leq M-1. \tag{13}$$

We introduce the updating gradient vector $\mathbf{g}_m(k)$ by

$$\mathbf{g}_m(k) = \lambda_m(k)\mathbf{g}_m(k-1) + \tilde{\mathbf{y}}_m(k)\xi_m^*(k)\ , \tag{14}$$

where $\xi_m^*(k)$ is the complex conjugate of the mixed-tone estimated error at symbol k for $m \in M$ as given in (13).

A procedure of an orthogonal gradient adaptive (OGA) algorithm to determine $\lambda_m(k)$ has been described in [17] by projecting the gradient vector $\mathbf{g}_m(k)$ onto the previous direction

vector $\mathbf{d}_m(k-1)$. This leads us to obtain the direction vector $\mathbf{d}_m(k)$.

By determining the direction vector $\mathbf{d}_m(k)$ through an orthogonal projection of the gradient vector $\mathbf{g}_m(k)$ onto the previous direction vector $\mathbf{d}_m(k-1)$, we arrive

$$\mathbf{d}_m(k) = \mathbf{g}_m(k) - \frac{\mathbf{d}_m(k-1)\,\mathbf{d}_m^H(k-1)}{\mathbf{d}_m^H(k-1)\,\mathbf{d}_m(k-1)}\mathbf{g}_m(k)\ . \tag{15}$$

Thus, $\mathbf{d}_m(k)$ is orthogonal to the previous direction vector $\mathbf{d}_m(k-1)$ weighted by the forgetting-factor $\lambda_m(k)$. We can easily optimise a value of $\lambda_m(k)$ based on a sample-by-sample basis by taking the previous direction vector $\mathbf{d}_m(k-1)$ in (11) and setting to zero as

$$\begin{aligned}\mathbf{d}_m^H(k)\mathbf{d}_m(k-1) &= \lambda_m(k)\mathbf{d}_m^H(k-1)\mathbf{d}_m(k-1) + \mathbf{g}_m^H(k)\mathbf{d}_m(k-1)\\ &= 0\ .\end{aligned} \tag{16}$$

Meanwhile, the gradient vector $\mathbf{g}_m(k)$ becomes the direction vector $\mathbf{d}_m(k)$ when the gradient vector $\mathbf{g}_m(k)$ is orthogonal to previous direction vector $\mathbf{d}_m(k-1)$ by $\mathbf{g}_m^H(k)\mathbf{d}_m(k-1) = 0$. The forgetting-factor parameter $\lambda_m(k)$ can be calculated for each tone m at symbol k as

$$\lambda_m(k) = \left| \frac{\mathbf{g}_m^H(k)\,\mathbf{d}_m(k-1)}{\mathbf{d}_m^H(k-1)\,\mathbf{d}_m(k-1)} \right|\ . \tag{17}$$

According to the results in [10], it is noticed that the results of FGA and OGA algorithms are similar to those obtained by the normalised version of OGA (NOGA) algorithm. The convergence rate of the NOGA algorithm is shown that it is better than that of both FGA and OGA.

Therefore, we introduce the mixed-tone normalised orthogonal gradient adaptive (MT-NOGA) algorithm which can be applied recursively as

$$\tilde{\mathbf{g}}_m(k) = \tilde{\lambda}_m(k)\,\tilde{\mathbf{g}}_m(k-1) + \frac{\tilde{\mathbf{y}}_m(k)\,\xi_m^*(k)}{\|\tilde{\mathbf{y}}_m(k)\|^2}\,, \tag{18}$$

$$\tilde{\lambda}_m(k) = \left| \frac{\tilde{\mathbf{g}}_m^H(k)\,\mathbf{d}_m(k-1)}{\mathbf{d}_m^H(k-1)\,\mathbf{d}_m(k-1)} \right|\ , \tag{19}$$

where $\tilde{\mathbf{g}}_m(k)$ is obtained instead of the gradient vector $\mathbf{g}_m(k)$ in (14) and (17) for this normalised version and $\xi_m^*(k)$ is the complex conjugate of the mixed-tone estimated error at symbol k for $m \in M$ as given in (13).

5.2. Adaptive step-size algorithms

This section describes the proposed low complexity adaptive step-size algorithms with the method of the mixed-tone criterion as described in Section 4 as follows.

http://dx.doi.org/10.5772/52158

5.2.1. Modified Adaptive Step-size algorithm (MAS)

Following [18] and [19], the step-size parameter is controlled by squared prediction mixed-tone error. If a large error will be the cause of increased step-size for fast tracking, while a small error will result in a decreased step-size to yield smaller misadjustment. This algorithm can be expressed as

$$\mu_m(k+1) = \gamma\, \mu_m(k) + \beta |\xi_m(k)|^2 \,, \tag{20}$$

where $0 \leq \gamma < 1$, $\beta > 0$ and $\xi_m(k)$ is the *a priori* mixed-tone estimated error at symbol k for $m \in M$ as given in (13).

We note that the instantaneous mixed-tone cost function controls the step-size parameter. This idea is that a large prediction error causes the step-size to increase and provides faster tracking, while a small prediction error will result in a decrease in the step-size to yield smaller misadjustment. The step-size parameter $\mu_m(k)$ at symbol k for $m \in M$ is always positive and is controlled by the size of the prediction error and parameters γ and β. The summary of proposed MAS-MTNOGA algorithm is presented in Table 1.

5.2.2. Adaptive Averaging Step-size algorithm (AAS)

The objective is to ensure large step-size parameter when the algorithm is far from an optimum point with the step-size parameter decreasing as we approach the optimum [15].

This algorithm achieves the objective using an estimate of the autocorrelation between $\xi_m(k)$ and $\xi_m(k-1)$ to control step-size update $\tilde{\mu}_m(k+1)$. The estimate of an averaging of $\xi_m(k) \cdot \xi_m(k-1)$ is introduced as

$$\tilde{\mu}_m(k+1) = \gamma\, \tilde{\mu}_m(k) + \beta\, |\hat{\xi}_m(k)|^2 \,, \tag{21}$$

$$\hat{\xi}_m(k) = \alpha\, \hat{\xi}_m(k-1) + (1-\alpha)|\xi_m^*(k) \cdot \xi_m(k-1)| \,, \tag{22}$$

where $0 \leq \gamma < 1$ and β is an independent variable for scaling the prediction error. The exponentially weighting parameter α should be close to 1. The parameter $\xi_m^*(k)$ is the complex conjugate of the mixed-tone estimated error at symbol k for $m \in M$ as shown in (13). The use of $\hat{\xi}_m(k)$ responds to two objectives as presented in [15]. First, the error autocorrelation is generally a good measure for the optimum. Second, it rejects the effect of the uncorrelated noise sequence on the update step-size. The summary of proposed AAS-MTNOGA algorithm is presented in Table 2.

6. Computational complexity

In this section, we investigate the additional computational complexity of the proposed low complexity MAS and AAS algorithms. We consider that a multiplication of two complex numbers is counted as 4-real multiplications and 2-real additions. A multiplication of a real number with a complex number is computed by 2-real multiplications.

- Starting with soft-constrained initialisation as :
  $\hat{\mathbf{p}}_m(0) = \mathbf{0}; \Pi_m^{\perp}(0) = \mathbf{I}; \tilde{\mathbf{d}}_m(0) = \tilde{\mathbf{g}}_m(0) = [1\ 0\ \cdots\ 0]^T$.
- Do for $n \in N_d \quad n = 1, 2, \ldots,$ compute.
  for $\quad m = 1, 2, \ldots, M.$
  for $\quad k = 1, 2, \ldots, K.$

1. To compute $\hat{\mathbf{p}}_m(k)$ as:

$$\begin{aligned}
\hat{\mathbf{p}}_m(k) &= \hat{\mathbf{p}}_m(k-1) + \mu_m(k)\, \tilde{\mathbf{d}}_m(k)\ , \\
\tilde{\mathbf{d}}_m(k) &= \tilde{\lambda}_m(k)\, \tilde{\mathbf{d}}_m(k-1) + \tilde{\mathbf{g}}_m(k) \\
\tilde{\mathbf{g}}_m(k) &= \tilde{\lambda}_m(k)\, \tilde{\mathbf{g}}_m(k-1) + \frac{\tilde{\mathbf{y}}_m(k)\, \xi_m^*(k)}{\|\tilde{\mathbf{y}}_m(k)\|^2}\ , \\
\text{where} \quad \tilde{\lambda}_m(k) &= \left| \frac{\tilde{\mathbf{g}}_m^H(k)\, \tilde{\mathbf{d}}_m(k-1)}{\tilde{\mathbf{d}}_m^H(k-1)\, \tilde{\mathbf{d}}_m(k-1)} \right| .
\end{aligned}$$

2. To compute $\mu_m(k)$ as:

$$\begin{aligned}
\mu_m(k) &= \gamma\, \mu_m(k-1) + \beta\, |\xi_m(k-1)|^2\ , \\
\text{where} \quad \xi_m(k) &= \tilde{x}_m(k) - \hat{\mathbf{p}}_m^H(k-1)\tilde{\mathbf{y}}_m(k) - \sum_{l=1}^{L} \left(\Pi_l^{\perp}(k)\hat{\mathbf{p}}_l(k)\right)^H \tilde{\mathbf{y}}_l(k)\ , \\
&\qquad\qquad \text{for } m \neq l\ ,\ L \leq M-1. \\
\Pi_m^{\perp}(k) &= \tilde{\mathbf{I}} - \hat{\mathbf{p}}_m(k)\, [\hat{\mathbf{p}}_m^H(k)\, \hat{\mathbf{p}}_m(k)]^{-1}\, \hat{\mathbf{p}}_m^H(k)\ .
\end{aligned}$$

end
end
end

Table 1. Summary of the proposed modified adaptive step-size mixed-tone normalised orthogonal gradient adaptive (MAS-MTNOGA) PTEQs.

The proposed AAS mechanism involves two additional updates (21) and (22) as while the proposed MAS approach employs only one update (20) compared with the MT-NOGA algorithm in [11].

Therefore, the computational complexity of the proposed MAS-MTNOGA, AAS-MTNOGA and FS-MTNOGA algorithms are listed in Table 3, where $\mathbb{T}$ is the number of taps of PTEQ. It is shown that the proposed algorithms require a few additional number of operations.

http://dx.doi.org/10.5772/52158

- Starting with soft-constrained initialisation as :
  $\hat{\mathbf{p}}_m(0) = \mathbf{0}; \Pi_m^{\perp}(0) = \mathbf{I}; \tilde{\mathbf{d}}_m(0) = \tilde{\mathbf{g}}_m(0) = [1\ 0\ \cdots\ 0]^T$.
- Do for $n \in N_d \quad n = 1, 2, \ldots,$ compute.
  for $\quad m = 1, 2, \ldots, M.$
  for $\quad k = 1, 2, \ldots, K.$

1. To compute $\hat{\mathbf{p}}_m(k)$ as:

$$\begin{aligned}
\hat{\mathbf{p}}_m(k) &= \hat{\mathbf{p}}_m(k-1) + \tilde{\mu}_m(k)\, \tilde{\mathbf{d}}_m(k)\ , \\
\tilde{\mathbf{d}}_m(k) &= \tilde{\lambda}_m(k)\, \tilde{\mathbf{d}}_m(k-1) + \tilde{\mathbf{g}}_m(k) \\
\tilde{\mathbf{g}}_m(k) &= \tilde{\lambda}_m(k)\, \tilde{\mathbf{g}}_m(k-1) + \frac{\tilde{\mathbf{y}}_m(k)\, \xi_m^*(k)}{\|\tilde{\mathbf{y}}_m(k)\|^2}\ , \\
\text{where} \quad \tilde{\lambda}_m(k) &= \left| \frac{\tilde{\mathbf{g}}_m^H(k)\, \tilde{\mathbf{d}}_m(k-1)}{\tilde{\mathbf{d}}_m^H(k-1)\, \tilde{\mathbf{d}}_m(k-1)} \right| .
\end{aligned}$$

2. To compute $\tilde{\mu}_m(k)$ as:

$$\begin{aligned}
\tilde{\mu}_m(k) &= \gamma\, \tilde{\mu}_m(k-1) + \beta\, |\hat{\xi}_m(k-1)|^2\ , \\
\hat{\xi}_m(k) &= \alpha\, \hat{\xi}_m(k-1) + (1-\alpha) |\xi_m^*(k) \cdot \xi_m(k-1)|\ , \\
\text{where} \quad \xi_m(k) &= \tilde{x}_m(k) - \hat{\mathbf{p}}_m^H(k-1) \tilde{\mathbf{y}}_m(k) - \sum_{l=1}^{L} \left(\Pi_l^{\perp}(k) \hat{\mathbf{p}}_l(k) \right)^H \tilde{\mathbf{y}}_l(k)\ , \\
&\qquad\qquad \text{for } m \neq l\ ,\ L \leq M-1. \\
\Pi_m^{\perp}(k) &= \tilde{\mathbf{I}} - \hat{\mathbf{p}}_m(k)\, [\hat{\mathbf{p}}_m^H(k)\, \hat{\mathbf{p}}_m(k)]^{-1}\, \hat{\mathbf{p}}_m^H(k)\ .
\end{aligned}$$

end
end
end

Table 2. Summary of the proposed adaptive averaging step-size mixed-tone normalised orthogonal gradient adaptive (AAS-MTNOGA) PTEQs.

Algorithm	Number of operations per symbol		
	Multiplications	Additions	Divisions
MAS-MTNOGA	$8\mathbb{T}+5$	$8\mathbb{T}+5$	1
AAS-MTNOGA	$8\mathbb{T}+8$	$8\mathbb{T}+6$	1
MTNOGA [11]	$8\mathbb{T}+2$	$8\mathbb{T}+4$	1

Table 3. The computational complexity per symbol [21].

7. Performance analysis

The convergence behaviour and stability analysis of the proposed MAS and AAS mechanisms are investigated based on the mixed-tone weight-estimated error. The convergence analysis of both MAS and AAS mechanisms are carried out and the steady-state and mean-square expressions of the step-size parameter relating the mean convergence factor as presented in [21] .

In the following analysis, we study the steady-state performance of the proposed MAS and AAS algorithms. We assume that these algortihms have converged.

7.1. Convergence analysis of the proposed MAS mechanism

Taking expectations on both sides of (20), the steady-state step-size arrives at

$$E\{\mu_m(k+1)\} = \gamma\, E\{\mu_m(k)\} + \beta\, E\{|\xi_m(k)|^2\}\ . \tag{23}$$

To facilitate the analysis, the proposed MAS mechanism is under a few assumptions.

Assumption (i). *We consider the steady-state value of* $E\{\mu_m(k+1)\}$ *by*

$$\begin{aligned}\lim_{k\to\infty} E\{\mu_m(k+1)\} &= \lim_{k\to\infty} E\{\mu_m(k)\} = E\{\mu_m(\infty)\}\ ,\\ \lim_{k\to\infty} E\{|\xi_m(k)|^2\} &= \xi_m^{min} + \xi_m^{ex}(\infty)\ ,\end{aligned}$$

where ξ_m^{min} *is the minimum mean square error (MMSE) and* $\xi_m^{ex}(\infty)$ *is the excess of mean square error (EMSE) related with the optimisation criterion in the steady-state condition.*

Applying assumption (i) to (23), we obtain

$$\begin{aligned}E\{\mu_m(\infty)\} &= \gamma\, E\{\mu_m(\infty)\} + \beta\, (\xi_m^{\min} + \xi_m^{\mathrm{ex}}(\infty))\\ (1-\gamma)\, E\{\mu_m(\infty)\} &= \beta\, (\xi_m^{\min} + \xi_m^{\mathrm{ex}}(\infty))\\ E\{\mu_m(\infty)\} &= \frac{\beta\, (\xi_m^{\min} + \xi_m^{\mathrm{ex}}(\infty))}{(1-\gamma)}\ .\end{aligned} \tag{24}$$

To simplify these expressions, let us consider another assumptions.

Assumption (ii). *Let us consider that for (24), where*

$$\xi_m^{min} + \xi_m^{ex}(\infty)\ \approx\ \xi_m^{min}\ ,$$

and

$$\left(\xi_m^{min} + \xi_m^{ex}(\infty)\right)^2\ \approx\ \left(\xi_m^{min}\right)^2\ .$$

We then assume that $\xi_m^{ex}(\infty) \ll \xi_m^{min}$*, when the algorithm is close to optimum.*

http://dx.doi.org/10.5772/52158

Employing assumption (ii) to (24), the steady-state step-size for the proposed MAS algorithm becomes

$$E\{\mu_m(\infty)\} \approx \frac{\beta\,(\xi_m^{\min})}{(1-\gamma)}\,. \tag{25}$$

It is noted that the steady-state performance of proposed MAS mechanism has derived in (25) for predicting in the steady-state condition.

7.2. Convergence analysis of the proposed AAS mechanism

Following [20] and [22], the average estimate $\hat{\xi}_m(k)$ in (22) can be rewritten as

$$\hat{\xi}_m(k) = (1-\alpha)\sum_{i=0}^{k-1}\alpha^i\,\xi_m^*(k-i)\cdot\xi_m(k-i-1)\,. \tag{26}$$

and

$$|\hat{\xi}_m(k)|^2 = (1-\alpha)^2\sum_{i=0}^{k-1}\sum_{j=0}^{k-1}\alpha^i\,\alpha^j\,\xi_m^*(k-i)\cdot\xi_m(k-i-1)\cdot\xi_m^*(k-j)\cdot\xi_m(k-j-1)\,. \tag{27}$$

We assume that the proposed algorithm has converged in the steady-state condition. Also, the expectation of (27) can be expressed as

$$E\{|\hat{\xi}_m(k)|^2\} = (1-\alpha)^2\sum_{i=0}^{k-1}\alpha^{2i}\,E\{|\xi_m(k-i)|^2\}\cdot E\{|\xi_m(k-i-1)|^2\}\,, \tag{28}$$

where α is an exponential weighting parameter.

Using assumption (i) into (28), we have

$$E\{|\hat{\xi}_m(k)|^2\} = (1-\alpha)^2\,(1+\alpha^2+\alpha^4+\cdots+\alpha^{2k})\cdot(\xi_m^{\min}+\xi_m^{\mathrm{ex}}(\infty))^2\,. \tag{29}$$

For convenience of computation, let

$$E\{|\hat{\xi}_m(k)|^2\} = (1-\alpha)^2\,\mathcal{A}\,, \tag{30}$$

where

$$\mathcal{A} = (1+\alpha^2+\alpha^4+\cdots+\alpha^{2k})\cdot(\xi_m^{\min}+\xi_m^{\mathrm{ex}}(\infty))^2\,. \tag{31}$$

By multiplying α^2 on both sides of $\mathcal{A}$ in (31), if $k \to \infty$ and $0 < \alpha < 1$, we get

$$\begin{aligned}\alpha^2\,\mathcal{A} &= \alpha^2 \cdot (1 + \alpha^2 + \alpha^4 + \ldots + \alpha^{2(k-1)} + \alpha^{2k}) \cdot (\xi_m^{\min} + \xi_m^{\text{ex}}(\infty))^2 \\ &= (\alpha^2 + \alpha^4 + \alpha^6 + \ldots + \alpha^{2(k-1)} + \alpha^{2k}) \cdot (\xi_m^{\min} + \xi_m^{\text{ex}}(\infty))^2 \\ &= \mathcal{A} - (\xi_m^{\min} + \xi_m^{\text{ex}}(\infty))^2 \,. \end{aligned} \tag{32}$$

Rearranging (32) to get $\mathcal{A}$, we arrive at

$$\begin{aligned}(1 - \alpha^2) \cdot \mathcal{A} &= (\xi_m^{\min} + \xi_m^{\text{ex}}(\infty))^2 \\ \mathcal{A} &= \frac{(\xi_m^{\min} + \xi_m^{\text{ex}}(\infty))^2}{(1 - \alpha^2)} \,. \end{aligned} \tag{33}$$

Substituting (33) into (30), we get

$$\begin{aligned}E\{|\hat{\xi}_m(k)|^2\} &= \frac{(1-\alpha)^2 \cdot (\xi_m^{\min} + \xi_m^{\text{ex}}(\infty))^2}{(1 - \alpha^2)} \\ &= \frac{(1-\alpha) \cdot (1-\alpha) \cdot (\xi_m^{\min} + \xi_m^{\text{ex}}(\infty))^2}{(1+\alpha) \cdot (1-\alpha))} \\ &= \frac{(1-\alpha) \cdot (\xi_m^{\min} + \xi_m^{\text{ex}}(\infty))^2}{(1+\alpha)} \,. \end{aligned} \tag{34}$$

Taking the expectation on both sides of (21), the mean behaviour of step-size $\tilde{\mu}_m(k)$ is given as

$$E\{\tilde{\mu}_m(k+1)\} = \gamma\, E\{\tilde{\mu}_m(k)\} + \beta\, E\{|\hat{\xi}_m(k)|^2\} \,. \tag{35}$$

Using assumption (i) and (34) into (35), we get

$$\begin{aligned}E\{\tilde{\mu}_m(\infty)\} &= \gamma\, E\{\tilde{\mu}_m(\infty)\} + \frac{\beta\,(1-\alpha) \cdot (\xi_m^{\min} + \xi_m^{\text{ex}}(\infty))^2}{(1+\alpha)} \\ (1-\gamma) \cdot E\{\tilde{\mu}_m(\infty)\} &= \frac{\beta\,(1-\alpha) \cdot (\xi_m^{\min} + \xi_m^{\text{ex}}(\infty))^2}{(1+\alpha)} \\ E\{\tilde{\mu}_m(\infty)\} &= \frac{\beta\,(1-\alpha) \cdot (\xi_m^{\min} + \xi_m^{\text{ex}}(\infty))^2}{(1-\gamma) \cdot (1+\alpha)} \,. \end{aligned} \tag{36}$$

where $\xi_m^{\min}$ is the steady-state minimum value and $\xi_m^{\text{ex}}(\infty)$ is the steady-state excess error of mixed-tone cost function.

http://dx.doi.org/10.5772/52158

By using assumption (ii), the steady-state value of $E\{\tilde{\mu}_m(\infty)\}$ in (36) is approximately as

$$E\{\tilde{\mu}_m(\infty)\} \approx \frac{\beta\,(1-\alpha)\cdot\left(\xi_m^{\min}\right)^2}{(1-\gamma)\cdot(1+\alpha)}\ . \tag{37}$$

We note that (37) has proven for predicting the steady-state performance of proposed AAS algorithm.

7.3. Stability and performance analysis

We introduce the stability and performance analysis of proposed algorithm that is based on the mean-square value of the mixed-tone estimated $\xi_m(k)$.

Let us denote the weight-error vector $\boldsymbol{\varepsilon}_m(k)$ at symbol k for each tone m by following [23] and [24]

$$\boldsymbol{\varepsilon}_m(k) = \mathbf{p}_{opt,m} - \hat{\mathbf{p}}_m(k)\ , \tag{38}$$

where $\mathbf{p}_{\mathrm{opt},m}$ denotes as the optimum Wiener solution for the tap-weight vector.

The estimate tap-weight PTEQ vector $\hat{\mathbf{p}}_m(k)$ can be introduced as

$$\hat{\mathbf{p}}_m(k) = \hat{\mathbf{p}}_m(k-1) + \mu_m(k)\sum_{i=1}^{k}\lambda^{k-i}\frac{\tilde{\mathbf{y}}_m(i)\,\xi_m^*(i)}{\|\tilde{\mathbf{y}}_m^H(i)\,\tilde{\mathbf{y}}_m(i)\|}\ , \tag{39}$$

where $\xi_m(k)$ is the *a priori* mixed-tone estimated error at symbol k for tone m as

$$\xi_m(k) = \tilde{x}_m(k) - \hat{\mathbf{p}}_m^H(k-1)\tilde{\mathbf{y}}_m(k) - \sum_{l=1}^{L}(\Pi_l^{\perp}(k)\hat{\mathbf{p}}_l(k))^H\tilde{\mathbf{y}}_l(k)\ .$$
$$\text{for } m \neq l\ , L \leq M-1 \tag{40}$$

Subtracting $\mathbf{p}_{\mathrm{opt},m}$ from both sides of (39) and using (40) to eliminate $\hat{\mathbf{p}}_m(k)$, we may rewrite as

$$\begin{aligned}\mathbf{p}_{opt,m} - \hat{\mathbf{p}}_m(k) = \mathbf{p}_{opt,m} - \hat{\mathbf{p}}_m(k-1) + \mu_m(k)\sum_{i=1}^{k}\lambda^{k-i}\frac{\tilde{\mathbf{y}}_m(i)}{\|\tilde{\mathbf{y}}_m^H(i)\tilde{\mathbf{y}}_m(i)\|}\Bigg\{\tilde{x}_m(i) - \hat{\mathbf{p}}_m^H(k-1)\tilde{\mathbf{y}}_m(i)\\ - \sum_{l=1}^{L}(\Pi_l^{\perp}(i)\hat{\mathbf{p}}_l(k))^H\tilde{\mathbf{y}}_l(i)\Bigg\}^* + \mu_m(k)\sum_{i=1}^{k}\lambda^{k-i}\frac{\tilde{\mathbf{y}}_m(i)}{\|\tilde{\mathbf{y}}_m^H(i)\tilde{\mathbf{y}}_m(i)\|}\left(\mathbf{p}_{opt,m}^H\tilde{\mathbf{y}}_m(i)\right)^*\\ - \mu_m(k)\sum_{i=1}^{k}\lambda^{k-i}\frac{\tilde{\mathbf{y}}_m(i)}{\|\tilde{\mathbf{y}}_m^H(i)\tilde{\mathbf{y}}_m(i)\|}\left(\mathbf{p}_{opt,m}^H\tilde{\mathbf{y}}_m(i)\right)^*\ .\end{aligned} \tag{41}$$

Substituting (38) in (41), we get

$$\boldsymbol{\varepsilon}_m(k) = \boldsymbol{\varepsilon}_m(k-1) - \mu_m(k) \sum_{i=1}^{k} \lambda^{k-i} \frac{\tilde{\mathbf{y}}_m(i)\tilde{\mathbf{y}}_m^H(i)\boldsymbol{\varepsilon}_m(k-1)}{\|\tilde{\mathbf{y}}_m^H(i)\tilde{\mathbf{y}}_m(i)\|} + \mu_m(k) \sum_{i=1}^{k} \lambda^{k-i} \frac{\tilde{\mathbf{y}}_m(i)}{\|\tilde{\mathbf{y}}_m^H(i)\tilde{\mathbf{y}}_m(i)\|} \left\{ \tilde{x}_m(i) - \mathbf{p}_{\text{opt},m}^H \tilde{\mathbf{y}}_m(i) - \sum_{l=1}^{L} (\Pi_l^{\perp}(i)\hat{\mathbf{p}}_l(k))^H \tilde{\mathbf{y}}_l(i) \right\}^* . \tag{42}$$

Then, the weight-error vector $\boldsymbol{\varepsilon}_m(k)$ can be expressed as

$$\boldsymbol{\varepsilon}_m(k) = \left[\mathbf{I} - \mu_m(k) \sum_{i=1}^{k} \lambda^{k-i} \frac{\tilde{\mathbf{y}}_m(i)\tilde{\mathbf{y}}_m^H(i)}{\|\tilde{\mathbf{y}}_m^H(i)\tilde{\mathbf{y}}_m(i)\|} \right] \boldsymbol{\varepsilon}_m(k-1) + \mu_m(k) \sum_{i=1}^{k} \lambda^{k-i} \frac{\tilde{\mathbf{y}}_m(i)\ \xi_{\text{opt},m}^*}{\|\tilde{\mathbf{y}}_m^H(i)\tilde{\mathbf{y}}_m(i)\|} . \tag{43}$$

where $\xi_{\text{opt},m}^*$ is the complex conjugate of estimation mixed-tone error produced in the optimum Wiener solution as

$$\xi_{\text{opt},m} = \tilde{x}_m(i) - \mathbf{p}_{\text{opt},m}^H \tilde{\mathbf{y}}_m(i) - \sum_{l=1}^{L} (\Pi_l^{\perp}(i)\hat{\mathbf{p}}_l(k))^H \tilde{\mathbf{y}}_l(i) . \quad \text{for } m \neq l\ , L \leq M-1 \tag{44}$$

Assumption (iii). *We consider the condition necessary for the convergence of mean, that is*

$$E\{\ \|\boldsymbol{\varepsilon}_m(k)\|\ \} \to 0\ ,\ \ as\ \ k \to \infty$$

or equivalently,

$$E\{\ \hat{\boldsymbol{p}}_m(k)\ \} \to \boldsymbol{p}_{opt,m}\ ,\ \ as\ \ k \to \infty$$

where $\|\boldsymbol{\varepsilon}_m(k)\|$ is the Euclidean norm of the weight-error vector $\boldsymbol{\varepsilon}_m(k)$.

We denote the mixed-tone estimated error for tone m at symbol k as

$$\xi_m(k) = \tilde{x}_m(k) - \hat{\mathbf{p}}_m^H(k)\ \tilde{\mathbf{y}}_m(k) - \sum_{l=1}^{L} (\Pi_l^{\perp}(k)\hat{\mathbf{p}}_l(k))^H \tilde{\mathbf{y}}_l(k) . \quad \text{for } m \neq l\ , L \leq M-1 \tag{45}$$

Using (38) into (45), the estimation mixed-tone error $\xi_m(k)$ at symbol k for each tone m is given as in (46), where $\xi_{\text{opt},m}$ is the estimation mixed-tone error in the optimum Wiener

http://dx.doi.org/10.5772/52158

solution shown in (44).

$$\begin{aligned}\xi_m(k) &= \tilde{x}_m(k) - \hat{\mathbf{p}}_m^H(k)\,\tilde{\mathbf{y}}_m(k) - \sum_{l=1}^{L}(\Pi_l^{\perp}(k)\hat{\mathbf{p}}_l(k))^H\tilde{\mathbf{y}}_l(k)\\ &= \tilde{x}_m(k) - (\mathbf{p}_{\mathrm{opt},m} - \boldsymbol{\varepsilon}_m(k))^H\tilde{\mathbf{y}}_m(k) - \sum_{l=1}^{L}(\Pi_l^{\perp}(k)\hat{\mathbf{p}}_l(k))^H\,\tilde{\mathbf{y}}_l(k)\\ &= \tilde{x}_m(k) - \mathbf{p}_{\mathrm{opt},m}^H\,\tilde{\mathbf{y}}_m(k) - \sum_{l=1}^{L}(\Pi_l^{\perp}(k)\hat{\mathbf{p}}_l(k))^H\,\tilde{\mathbf{y}}_l(k) + \boldsymbol{\varepsilon}_m^H(k)\,\tilde{\mathbf{y}}_m(k)\\ &= \xi_{\mathrm{opt},m} + \boldsymbol{\varepsilon}_m^H(k)\,\tilde{\mathbf{y}}_m(k)\ . \end{aligned} \tag{46}$$

Let $\hat{J}_m(k)$ denotes as the expectation of mean square mixed-tone error at tone m for $m \in M$

$$\begin{aligned}\hat{J}_m(k) &= E\{\,|\xi_m(k)|^2\,\}\\ &= E\{\big(\xi_{\mathrm{opt},m} + \boldsymbol{\varepsilon}_m^H(k)\tilde{\mathbf{y}}_m(k)\big)^*\big(\xi_{\mathrm{opt},m} + \boldsymbol{\varepsilon}_m^H(k)\tilde{\mathbf{y}}_m(k)\big)\}\\ &= E\{|\xi_{\mathrm{opt},m}|^2\} + E\{\tilde{\mathbf{y}}_m^H(k)\boldsymbol{\varepsilon}_m(k)\xi_{\mathrm{opt},m}\}\\ &\qquad + E\{\boldsymbol{\varepsilon}_m^H(k)\tilde{\mathbf{y}}_m(k)\xi_{\mathrm{opt},m}^*\}\\ &\qquad + E\{\boldsymbol{\varepsilon}_m^H(k)\boldsymbol{\varepsilon}_m(k)\tilde{\mathbf{y}}_m^H(k)\tilde{\mathbf{y}}_m(k)\}\ . \end{aligned} \tag{47}$$

By using assumption (iii), we assume that

$$\hat{J}_m(k) = J_m^{min} + J_m^{ex}(k)\ , \tag{48}$$

where J_m^{min} is the minimum mean square mixed-tone error produced by the optimum Wiener filter for tone m as

$$J_m^{min}(k) = E\{|\xi_{\mathrm{opt},m}|^2\} + E\{\boldsymbol{\varepsilon}_m^H(k)\tilde{\mathbf{y}}_m(k)\xi_{\mathrm{opt},m}^*\} + E\{\tilde{\mathbf{y}}_m^H(k)\boldsymbol{\varepsilon}_m(k)\xi_{\mathrm{opt},m}\}\ , \tag{49}$$

and $J_m^{ex}(k)$ is called the excess mean square mixed-tone error (EMSE) at symbol k for tone m as

$$J_m^{ex}(k) = E\{\,\boldsymbol{\varepsilon}_m^H(k)\boldsymbol{\varepsilon}_m(k)\tilde{\mathbf{y}}_m^H(k)\tilde{\mathbf{y}}_m(k)\,\}\ . \tag{50}$$

Since

$$\mathcal{R}_{\tilde{\mathbf{y}}\tilde{\mathbf{y}}} = E\{\tilde{\mathbf{y}}_m(k)\,\tilde{\mathbf{y}}_m^H(k)\}\ , \tag{51}$$

and by the orthogonality principle

$$E\{\xi_{\mathrm{opt},m}\,\tilde{\mathbf{y}}_m(k)\} \approx 0\ , \tag{52}$$

the excess in mean square mixed-tone error is given by

$$J_m^{ex}(k) = E\{\, \boldsymbol{\varepsilon}_m^H(k)\, \mathcal{R}_{\tilde{\mathbf{y}}\tilde{\mathbf{y}}}\, \boldsymbol{\varepsilon}_m(k)\, \}\ . \tag{53}$$

where $\boldsymbol{\varepsilon}_m(k)$ denotes as the weight-error vector at symbol k for each tone m shown in (38).

8. Simulation results

In this section, we implemented transmission simulations for the ADSL-based downstream including additive white Gaussian noise (AWGN) and near-end crosstalk (NEXT) detailed as follows. The used tones for downstream transmission were starting at active tones 38 to 255 and unused tones including tones 8 to 32 for upstream transmission were set to zero. The samples of reference carrier serving area (CSA) loop were used for the entire test channel, which comprises 512 coefficients of channel impulse response. The ADSL downstream simulations with the CSA loop #4 was the representative of simulations with all 8 CSA loops detailed in [25] as follows. The CSA#4 loop is consisting of 26-gauge bridged tap of length of 400 ft. at 550 ft., of 800 ft. at 6800 ft. and 26-gauge loop of length of 800 ft. at 7600 ft., respectively. Other parameters were as the sampling rate $f_s = 2.208$ MHz and the size of FFT $N = 512$. The length of CP (ν) was identical to 32. The synchronisation delay was of 45. The SNR gap of 9.8dB, the coding gain of 4.2dB, the noise margin of 6 dB, and the input signal power of -40 dBm/Hz were used for all active tones [1]. With the power of AWGN of -140dBm/Hz and NEXT from 24 ADSL disturbers were included in the test channel. The bit allocation calculation requires an estimate of signal to noise ratio (SNR) on tone $n \in N_d$, when the noise energy is estimated after per-tone equalisation.

We compare the proposed MAS-MTNOGA and AAS-MTNOGA PTEQs with variable step-size parameters compared with the fixed step-size MT-NOGA [11] PTEQ. The proposed algorithms were initialised with $\mathbb{T} = 32, \hat{\mathbf{p}}_m(0) = [\,0\ 0\ 0\ \ldots\ \ 0\,]^T$, $\tilde{\mathbf{d}}_m(0) = \tilde{\mathbf{g}}_m(0) = [\,1\ 0\ 0\ \ldots\ \ 0\,]^T$ and $\Pi_m^{\perp}(0) = \mathbf{I}$, where $\lambda_m(0) = 0.95, \hat{\zeta}_m(0) = \sigma_\eta^2$. The matrix $\mathbf{I}$ is the identity matrix and the parameter σ_η^2 is the variance of AWGN and NEXT. We considered the use of the combining estimated of 3-adjacent tones $(M = 3)$. All the following results were obtained by averaging over 50 Monte Carlo trials.

Fig. 4 and Fig. 5 show the sum of squared mixed-tone errors learning curves of proposed AAS-MTNOGA, MAS-MTNOGA and MT-NOGA PTEQs are illustrated with the different values of fixed step-size parameters for the samples of the active tone at $m = 200$ and 250, respectively. It is observed that the proposed AAS-MTNOGA algorithm can converge more rapidly to steady-state condition than MT-NOGA with the fixed step-size. Learning curves of the excess mean square mixed-tone errors (EMSE) $J_m^{ex}(k)$ of proposed AAS-MTNOGA, MAS-MTNOGA and MT-NOGA PTEQs in Fig. 6 and Fig. 7 are depicted with the different values of fixed step-size parameters for the samples of the active tone at $m = 200$ and 250, respectively. Fig. 8 and Fig. 9 depict the trajectories of step-size parameters $\mu_m(k)$ of proposed MAS-MTNOGA and AAS-MTNOGA algorithms at different initial step-size settings with the sample of the active tone at $m = 250$, respectively. It is shown to converge to its own equilibrium despite large variations of initial step-size parameters.

http://dx.doi.org/10.5772/52158

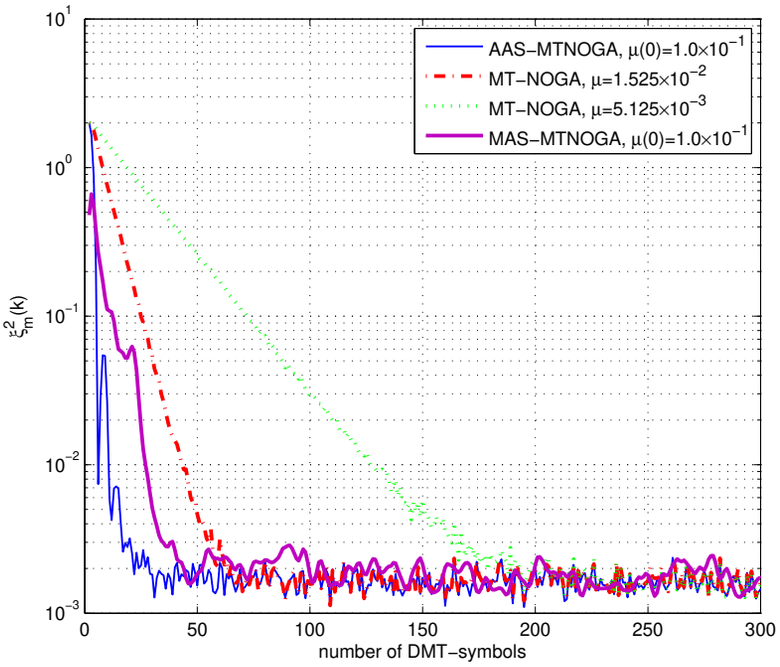

Figure 4. Learning curves of sum of squared mixed-tone errors of the proposed MAS-MTNOGA, AAS-MTNOGA and MTNOGA [11] algorithms with the sample of active tone $m = 200$. The other fixed parameters of the proposed ASS-MTNOGA algorithm are $\gamma = 0.985$, $\beta = 1.25 \times 10^{-2}$, and $\alpha = 0.995$.

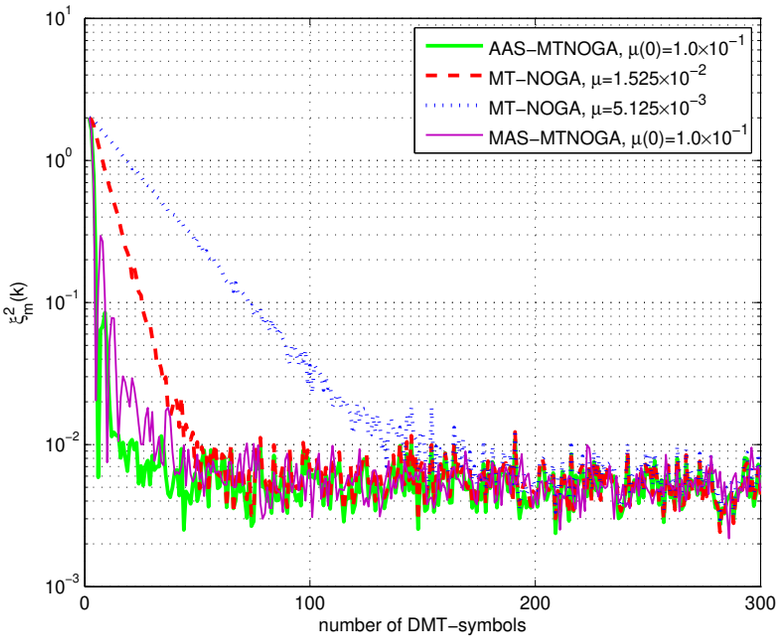

Figure 5. Learning curves of sum of squared mixed-tone errors of the proposed MAS-MTNOGA, AAS-MTNOGA and MTNOGA [11] algorithms with the sample of active tone $m = 250$. The other fixed parameters of the proposed ASS-MTNOGA algorithm are $\gamma = 0.985$, $\beta = 1.25 \times 10^{-2}$, and $\alpha = 0.995$.

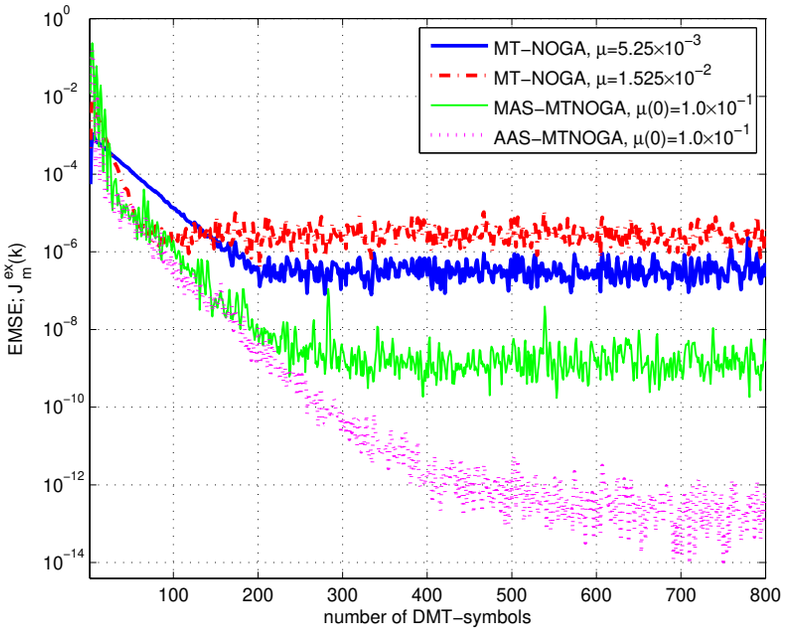

Figure 6. Learning curves of EMSE $J_m^{ex}(k)$ of the proposed MAS-MTNOGA, AAS-MTNOGA and MTNOGA [11] algorithms with the sample of active tone $m = 200$. The other fixed parameters of the proposed ASS-MTNOGA algorithm are $\gamma = 0.985$, $\beta = 1.25 \times 10^{-2}$, and $\alpha = 0.995$.

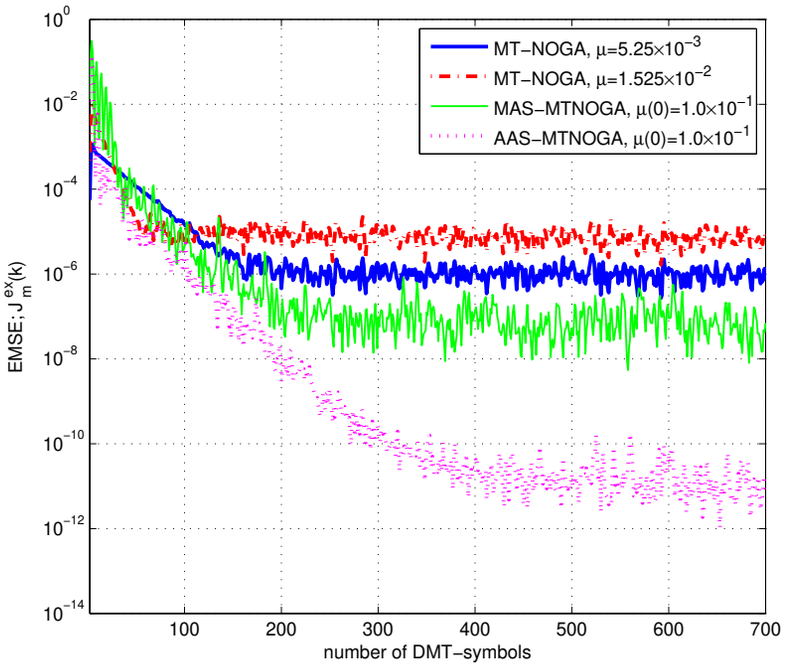

Figure 7. Learning curves of EMSE $J_m^{ex}(k)$ of the proposed MAS-MTNOGA, AAS-MTNOGA and MTNOGA [11] algorithms with the sample of active tone $m = 250$. The other fixed parameters of the proposed ASS-MTNOGA algorithm are $\gamma = 0.985$, $\beta = 1.25 \times 10^{-2}$, and $\alpha = 0.995$.

http://dx.doi.org/10.5772/52158

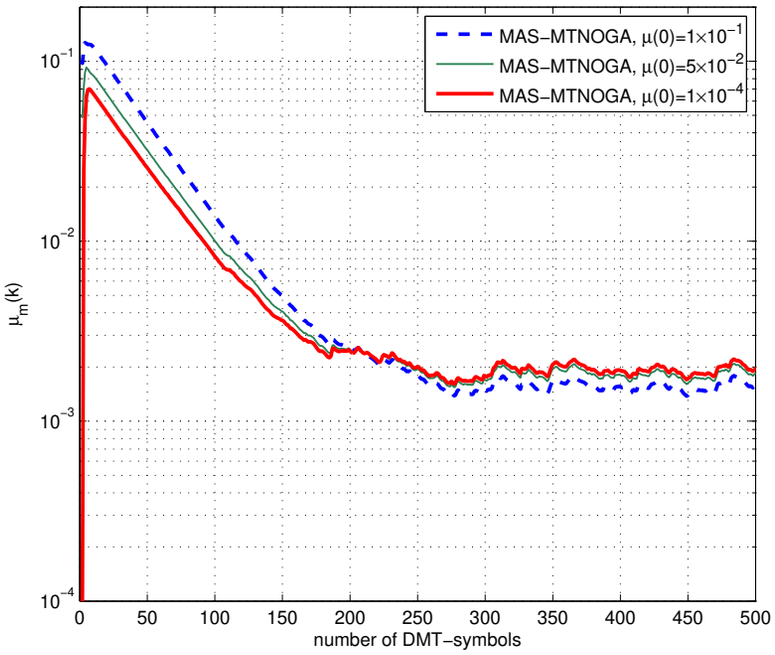

Figure 8. Trajectories of the adaptive step-size $\mu_m(k)$ of the proposed MAS-MTNOGA algorithm using different setting of $\mu(0) = 1 \times 10^{-1}, 5 \times 10^{-2}$ and 1×10^{-4} with the sample of active tone $m = 250$.

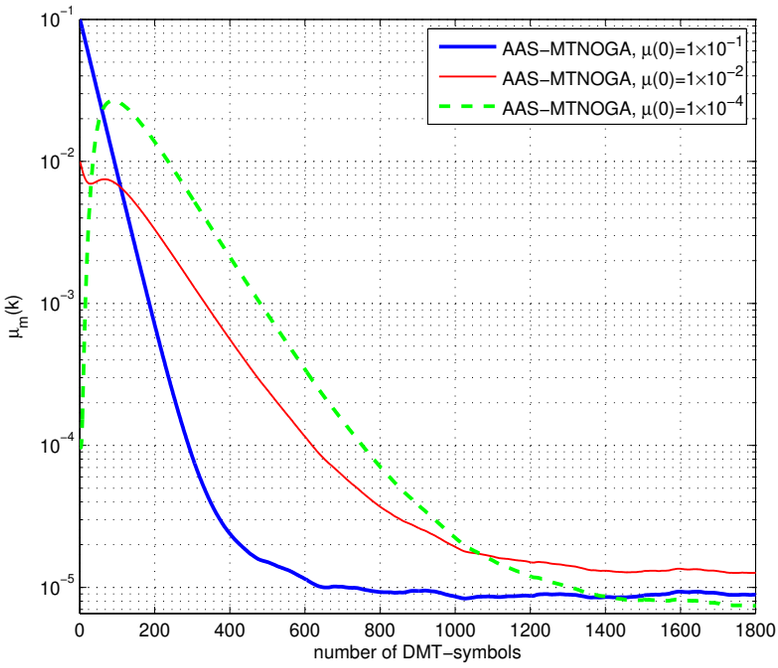

Figure 9. Trajectories of the adaptive step-size $\mu_m(k)$ of the proposed AAS-MTNOGA algorithm using different setting of $\mu(0) = 1 \times 10^{-1}, 1 \times 10^{-2}$ and 1×10^{-4} with the sample of active tone $m = 250$.

9. Conclusion

In this chapter, we present the proposed MAS-MTNOGA and AAS-MTNOGA algorithm for per-tone equalisation in DMT-based systems. We describe the tap-weight estimated PTEQ vector $\hat{\mathbf{p}}_m(k)$ for $m \in M$ of M-combining tones. The mixed-tone cost function is demonstrated as the sum of mixed-tone weight estimated errors of adjacent tones. With the method of adaptive step-size approach and the normalised orthogonal gradient adaptive algorithm, two of low complexity adaptive step-size mechanisms can be achieved for per-tone equalisation based on the mixed-tone criterion. The derivation and analysis of two low complexity adaptive step-size schemes are presented. The adaptation of mean square mixed-tone errors (MSE) and excess mean square mixed-tone errors (EMSE) curves of proposed MAS-MTNOGA and AAS-MTNOGA algorithms are shown to converge rapidly to steady-state condition in the simulated channel. According to simulation results, the proposed algorithms can provide the good performance and are appeared to be robust in AWGN and NEXT channel in comparison with the fixed step-size algorithm of MTNOGA algorithm.

Author details

Suchada Sitjongsataporn

Centre of Electronic Systems Design and Signal Processing (CESdSP),
Mahanakorn University of Technology, Thailand

References

[1] International Telecommunications Union (ITU). Recommendation G.996.1, *Test Procedures for Asymmetric Digital Subscriber Line (ADSL) Transceivers*, February 2001.

[2] International Telecommunications Union (ITU). Recommendation G.992.3, *Asymmetric Digital Subscriber Line (ADSL) Transceivers-2 (ADSL)*, July 2002.

[3] International Telecommunications Union (ITU). Recommendation G.992.5, *Asymmetric Digital Subscriber Line (ADSL) Transceivers-Extened Bandwidth ADSL2 (ADSL2+)*, May 2003.

[4] P.Golden, H.Dedieu, and K.S.Jacobsen, *Fundamentals of DSL Technology*, Auerbach Publications, Taylor&Francis Group, 2006.

[5] P.Golden, H.Dedieu, and K.S.Jacobsen, *Implementation and Applications of DSL Technology*, Auerbach Publications, Taylor&Francis Group, 2008.

[6] S.Sitjongsataporn and P.Yuvapoositanon, "Adaptive Step-size Order Statistic LMS-based Time-domain Equalisation in Discrete Multitone Systems", *Discrete Time Systems*, Mario Alberto Jordán (Ed.), ISBN: 978-953-307-200-5, InTech, April 2011, Available from: http://www.intechopen.com/articles/show/title/adaptive-step-size-order-statistic-lms-based-time-domain-equalisation-in-discrete-multitone-systems

[7] K.V.Acker, G.Leus, M.Moonen, O.van de Wiel and T.Pollet, "Per Tone Equalization for DMT-based Systems", *IEEE Transactions on Communications*, vol. 49, no. 1, pp. 109-119, Jan. 2001.

[8] S.Sitjongsataporn and P.Yuvapoositanon, "Bit Rate Maximising Per-Tone Equalisation with Adaptive Implementation for DMT-based Systems", *EURASIP Journal on Advances in Signal Processing*, vol. 2009, Article ID 380560, 13 pages, 2009. doi:10.1155/2009/380560.

[9] S.Sitjongsataporn and P.Yuvapoositanon, "A Mixed-Tone RLS Algorithm with Orthogonal Projection for Per-Tone DMT Equalisation", in *Proc. IEEE International Midwest Symposium on Circuits and Systems (MWSCAS)*, Knoxville, USA, pp. 942-945, Aug. 2008.

[10] J.A.Apolinário Jr., R.G.Alves, P.S.R.Diniz and M.N.Swamy, "Filtered Gradient Algorithm Applied to a Subband Adaptive Filter Structure", in *Proc. IEEE International Conference Acoustics, Speech, and Signal Processing (ICASSP)*, vol.6, pp. 3705-3708, May 2001.

[11] S.Sitjongsataporn and P.Yuvapoositanon, "Mixed-Tone Normalised Orthogonal Gradient Adaptive Per-Tone DMT Equalisation", in *Proc. IEEE International Conference on Electrical Engineering/Electronics, Computer, Telecommunications and Information Technology (ECTI-CON)*, Pattaya, Thailand, pp. 1151-1154, May 2009.

[12] S.Sitjongsataporn and P.Yuvapoositanon, "Low Complexity Adaptive Step-size Filtered Gradient-based Per-Tone DMT Equalisation", in *Proc. IEEE International Symposium on Circuits and Systems (ISCAS)*, Paris, France, pp. 2526-2529, May 2010.

[13] P.K.Pandey and M.Moonen, "Resource Allocation in ADSL Variable Length Per-Tone Equalizers", *IEEE Transanctions on Signal Processing*, vol. 56, no. 5, May 2008.

[14] G.Strang, *Linear Algebra and Its Applications*, Harcourt Brace Jovanovich, 1988.

[15] L.Wang, Y.Cai and R.C.de Lamare, "Low-Complexity Adaptive Step-Size Constrained Constant Modulus SG-based Algorithms for Blind Adaptive Beamforming", in *Proc. IEEE International Conference Acoustics, Speech, and Signal Processing (ICASSP)*, pp. 2593-2596, 2008.

[16] L.Wang, R.C.de Lamare and Y.Cai, "Low-Complexity Adaptive Step-Size Constrained Constant Modulus SG Algorithms for Adaptive Beamforming", *Signal Processing*, vol.89, pp. 2503-2513, 2009.

[17] J.S.Lim, "New Adaptive Filtering Algorithm Based on an Orthogonal Projection of Gradient Vectors", *IEEE Signal Processing Letters*, vol. 7, no. 11, pp. 314-316, Nov. 2000.

[18] R.C.de Lamare and R.Sampaio-Neto, "Low-Complexity Variable Step-Size Mechanisms for Stochastic Gradient Algorithms in Mimimum Variance CDMA Receivers", *IEEE Transactions on Signal Processing*, vol. 54, pp. 2302-2317, Jun. 2006.

[19] Y.Cai and R.C.de Lamare, "Low-complexity Variable Step-Size Mechanism for Code-Constrained Constant Modulus Stochastic Gradient Algorithms Applied to

CDMA Interference Suppression", *IEEE Transactions on Signal Processing*, vol. 57, no. 1, pp. 313-323, Jan. 2009.

[20] R.H.Kwong and E.W.Johnston, "A Variable Step Size LMS Algorithm", *IEEE Transactions on Signal Processing*, vol.40, no.7, pp. 1633-1642, July 1992.

[21] S.Sitjongsataporn, "Analysis of Low Complexity Adaptive Step-size Orthogonal Gradient-based FEQ for OFDM Systems", *ECTI Transactions on Computer and Information Technology (ECTI-CIT)*, vol. 5, no. 2, pp. 133-144, Nov. 2011.

[22] T.Aboulnasr, and K.Mayyas, "A Robust Variable Step-Size LMS-Type Algorithm: Analysis and Simulations", *IEEE Transactions on Signal Processing*, vol. 45, no. 3, pp. 631-639, Mar. 1997.

[23] P.S.R.Diniz, *Adaptive Filtering: Algorithms and Practical Implementation*, Springer, 2008.

[24] S.Haykin, *Adaptive Filter Theory*, Prentice Hall, 1996.

[25] N.Al-Dhahir and J.M.Cioffi, "Optimum Finite-Length Equalization for Multicarrier Transceivers", *IEEE Transactions on Communications*, vol. 44, pp. 56-64, Jan. 1996.